Analyst

ROYAL SOCIETY OF CHEMISTRY

PAPER

View Article Online
View Journal | View Issue

Cite this: *Analyst*, 2023, **148**, 4373

High wavenumber Raman spectroscopy for intraoperative assessment of breast tumour margins†

Jennifer Haskell, [a,b] Thomas Hubbard, [a,b] Claire Murray,[b] Benjamin Gardner, [a,b] Charlotte Ives,[a,b] Douglas Ferguson [a,b] and Nick Stone *[a,b]

Optimal oncological results and patient outcomes are achieved in surgery for early breast cancer with breast conserving surgery (BCS) where this is appropriate. A limitation of BCS occurs when cancer is present at, or close, to the resection margin – termed a 'positive' margin – and re-excision is recommended to reduce recurrence rate. This is occurs in 17% of BCS in the UK and there is therefore a critical need for a way to assess margin status intraoperatively to ensure complete excision with adequate margins at the first operation. This study presents the potential of high wavenumber (HWN) Raman spectroscopy to address this. Freshly excised specimens from thirty patients undergoing surgery for breast cancer were measured using a surface Raman probe, and a multivariate classification model to predict normal *versus* tumour was developed from the data. This model achieved 77.1% sensitivity and 90.8% specificity following leave one patient out cross validation, with the defining features being differences in water content and lipid *versus* protein content. This demonstrates the feasibility of HWN Raman spectroscopy to facilitate future intraoperative margin assessment at specific locations. Clinical utility of the approach will require further research.

Received 12th April 2023,
Accepted 27th July 2023

DOI: 10.1039/d3an00574g

rsc.li/analyst

Introduction

Primary surgery and tumour excision remains the standard first line of treatment for patients with early breast cancer. Breast conserving surgery, (BCS), combined with radiotherapy, where the tumour is removed by wide local excision (lumpectomy) with a margin of surrounding healthy tissue, is oncologically equivalent to mastectomy (removal of the whole breast)[1] and is the preferred option where possible. Unlike mastectomy, this allows the patient to retain the majority of their breast tissue for much improved aesthetic and psychological outcomes.[2,3] However, with breast conserving surgery comes the problem of positive tumour margins, where the tumour is very close to the edge of the removed tissue, increasing the potential for abnormal tissue to remain behind. The current UK protocol requires a clear margin of 1 mm of healthy tissue to be removed around the entirety of the tumour.[4]

According to a *meta*-analysis of 28 162 women undergoing breast conserving surgery, local recurrence is twice as likely when margins are positive.[5] The current protocol[6,7] for locating the tumour on a macroscopic level involves palpation by the surgeon, and specimen radiograph for non-palpable tumours, but the only way to conclusively assess margins is through histopathological assessment, the results of which are not available until days or weeks after the operation.[8] Therefore, patients often need follow up surgery to re-excise any remaining tumour. In the UK, on average 17.2% of patients undergo re-excision operations, but this can be as high as 40% in some individual hospital units.[7] This comes at significant financial cost, as well as all the risks associated with additional surgery for the patient including, morbidity, anxiety, prolonged wound healing, infection and worse cosmetic outcome.[7,9] Therefore, a method which can assess tumour margins intraoperatively is needed.

There are currently many different approaches being researched within the field to try to achieve this. Frozen section analysis (FSA) and imprint cytology (IC) allow intraoperative assessment of the resected specimen by pathologists, and both methods have been proven to reduce re-excision rates.[10,11] However FSA tends add about 30 minutes on average to the operation time,[10,12] and breast tissue is difficult to cryosection due to its adiposity.[10,13] IC by contrast only takes about 15 minutes,[12] but at the expense of sensitivity,[10] with only the very surface layer of cells being assessed.[10] And with this, both methods require pathologists' time and are subject to sampling errors.[10,13]

Alternatives include imaging modalities such as ultrasound (US) and micro-CT. A review by Colakovic *et al.* of 16 studies

[a]*Physics and Astronomy, Faculty of Environment, Science and Economy, University of Exeter, Exeter, Devon, UK. E-mail: n.stone@exeter.ac.uk*
[b]*Royal Devon University Healthcare NHS Foundation Trust, Exeter, Devon, UK*
† Electronic supplementary information (ESI) available. See DOI: https://doi.org/10.1039/d3an00574g

showed that on average US guided resection achieved negative margins 86% of the time, with an average re-excision rate of 9%; compared to 24% for wire guided localisations (of those studies reporting this value).[14] Yet, a large proportion of patients may be unsuitable for this; ductal carcinoma *in situ* (DCIS) is often identified by calcifications, and due to their acoustic properties, US cannot reliably detect them.[15–17] This is not a problem with micro-CT, using and this method specimens can be assessed within 15 minutes, with a spatial resolution reported as <1 μm.[15,18] Yet there are only limited studies assessing this method's capability for assessing margins; Qiu *et al*. suggest in one of their studies that were the method used to directly inform the necessity of re-excision, rates would have been reduced from 32% to 14%, despite the same study only achieving 56% sensitivity.[18] It is also acknowledged that the diagnostic performance of X-rays is reduced with higher density tissue.[15]

Photoacoustic imaging is a newer technique that has been applied to breast cancer. This technique works through the generation and detection of acoustic waves from tissue when it undergoes themoelastic expansion following the application of a pulsed laser beam.[19] Through haemoglobin targeting, this technique has allowed the detection of malignant breast lesions through cancer induced angiogenesis.[20] More recently, lipids and collagen have been mapped using optoacoustic tomography in *ex vivo* breast tissue, which could provide new ways to detect and localise breast tumours.[21] Specifically, Kosik *et al*. developed a lipid-weighted Intraoperative Photoacoustic Screening scanner, which was used to measure breast lumpectomy specimens. The tumour volumes determined by the system showed a significant positive correlation and were statistically similar to that determined by dynamic contrast enhanced magnetic resonance imaging.[20] The specimen scans were completed in a clinically feasible time of only 6 minutes,[20] with depths greater than 2 cm achievable, helped by the fact that acoustic waves are less scattered in tissues than optical photons.[19,20] However, pressure was required to enable measurement of the lumpectomy samples to maximise laser fluence at increased depths; this may be the reason for the 5.1 cm average overestimate in maximum tumour diameter.[20]

Exploration in this field has yielded several commercially available products using different methods to address the problem. These include the iKnife, MarginProbe and ClearEdge, where the former utilises mass spectrometry, while the latter two systems make use of bio-impedance spectroscopy through slightly varied approaches.[22,23] The iKnife has the benefit that it integrates easily into current surgical practice, and it achieves high sensitivity and specificity (94.9% and 93.4% respectively),[22] rivalling if not improving upon the more traditional methods. Its resolution is limited, however, to 4 mm which is the width of the blade used.[22] Furthermore, it entirely destroys the tissue it samples, making validation of the result difficult. The MarginProbe® on the other hand is the only intraoperative margin assessment device currently approved by the Food and Drug Administration (FDA).[15] While it is frequently reported to significantly reduce re-excision rates,[24–26] and only takes 5 minutes to assess a specimen,[27] the sensitivity and specificity levels achieved tend to be reduced compared to other methods discussed. For example, in a study of 596 patients, Schnabel *et al*. demonstrate a sensitivity and specificity of margin assessment as 75% and 46% respectively, with deliberate tuning of the classification model to sacrifice specificity for enhanced sensitivity.[25] In comparison, the ClearEdge system reportedly achieves better sensitivity and specificity (87.3% and 75.6%) for assessing margins, and has the added advantage that it can be tuned to probe a particular depth within the specimen, *e.g.* 2 mm.[23] Dixon *et al*. found that re-excision rates were reduced from 37% to 17% using ClearEdge,[23] but there is currently little other literature to corroborate this, and the re-excision rate was reduced to the UK average from a comparatively high baseline.

Raman spectroscopy provides another different approach to the problem. Chemical information is obtained through the change of energy, or frequency shift, of light photons when they interact inelastically with molecular bonds. This shift is chemically specific, producing a spectrum of peaks corresponding to the bonds present in a tissue sample, *i.e.* a 'spectral fingerprint'. The technique has been used in several forms to successfully discriminate various forms of cancer.[28–31] Measuring fresh frozen *ex vivo* breast samples with a Raman microscope, Haka *et al*. characterised normal tissue, invasive carcinoma and benign fibrocystic change with a sensitivity of 94% and specificity of 96%,[28] but the protocol used here would take too long with necessary sampling to be feasible for margin assessment. The group then used this database to characterise new measurements of breast tissue margins taken with a Raman probe intraoperatively.[32] While this achieved perfect sensitivity and specificity values, the sample size is very small – 30 spectra from nine patients – and only one measurement turned out to be positive for cancer.[32]

Raman has also been demonstrated to be feasible for intraoperative identification of lymph node involvement in both breast cancer surgery[33,34] and for identifying primary and secondary cancers in head and neck surgery.[35] All of these studies utilise the fingerprint region of the spectrum, complex but rich in molecular information on the phenotypic cellular molecular composition.

There are a number of studies that have demonstrated that water concentration is increased in cancerous tissues. The first study to identify this was conducted by Damadian in 1971. Using nuclear magnetic resonance (NMR) on rat models with sarcoma and hepatoma, prolonged relaxation times of water protons in malignant tissue compared to normal tissue were observed.[36] Further NMR studies have confirmed this finding, again in rat and mouse models,[37] and a small number of human samples,[38] with relaxation times correlating with an increase in the hydration of the malignant tissue.[37] This has been demonstrated specifically in breast cancer, with tumour tissue measured to contain a higher water-fat ratio than normal tissue.[39,40] Corroborating this further are studies utilising diffuse optical spectroscopy (DOS), which when used *in vivo* indicated that malignant

breast tissue contained 20% reduced lipid content and about 50% increased water.[41]

The Raman fingerprint (FP) region is unsuitable for water analysis with low signals dominated by other molecular species, but the high wavenumber (HWN) region is very sensitive to water. In fact, some studies have demonstrated dual illumination methods to measure both the HWN region and the FP region for the extra information that lies there. Qi *et al.* demonstrated the use of a Raman probe with simultaneous laser excitation at both 681 nm and 785 nm for HWN and FP region measurement respectively, with the collected signal being decoupled by an algorithm the group devised. From the HWN spectra, they could ascertain water content of *in vivo* skin.[42] Similarly, Masson *et al.* used a Raman probe with dual laser excitation which could switch between 680 nm and 785 nm. From the HWN water band they were able to quantify the water content of tissue phantoms as well as from *ex vivo* mouse cervix tissue in different conformations validated by the wet and dry weights of the samples.[43] Assessing the HWN region only, a Raman probe was applied intraoperatively for margin analysis in oral cancer by Barroso *et al.*[44] While their work was not used to influence resection rates, it achieved a sensitivity of 99% and specificity of 92% based on the difference in water content of normal *versus* cancerous tissue, which was stark ($p < 0.0001$).[44] Using this principle, the group later demonstrated how water levels decrease with distance across margins, starting high within the tumour and decreasing across an inadequate margin, and decreasing further towards an adequate margin.[45] Several studies utilising the HWN region have also found water content to be higher in cancerous *versus* non-cancerous breast tissue. This includes samples from rat models[46] and snap frozen – defrosted human samples.[47] The latter, undertaken by Hubbard *et al.*, was important in establishing that fluorescence from surgical dye used routinely in breast surgery can be minimised by measuring the HWN region at a longer illumination wavelength of 785 nm.[47] But due to the reduced quantum efficiency of CCDs in the HWN region at this wavelength, it was necessary to use an InGaAs camera instead, unlike in the previously mentioned studies by Qi, Masson, and Barroso *et al.* Abramczyk *et al.* successfully discerned normal from tumour in fresh breast samples using HWN Raman spectroscopy, but their protocol involved taking thousands of spectra using a Raman microscope, which would take too long to implement intraoperatively.[48] To improve on the preliminary work by Hubbard *et al.*, fresh samples should be measured. Yet, along with the work by Barroso *et al.* and Hubbard *et al.*, the study convincingly proves the potential of this approach for assessing breast margins. The HWN spectrum has also been used as a screening tool, by Liao *et al.*, to identify suspicious areas followed by definitive assessment with the FP region,[49] however, in this study the water peak between 3035–3680 cm^{-1} was not included in the analysis, and the diagnostic ability of HWN RS for breast cancer remains under investigated. Therefore, the following study aims to establish whether HWN Raman spectroscopy using a handheld Raman probe can discern tumour *versus* non-tumour status in *ex vivo* fresh breast tissue with measurements taken in a clinically relevant setting and timeframe.

Materials and methods

Tissue samples

Tissue specimens resected as part of standard oncological resection from 30 patients were measured at the Royal Devon and Exeter Hospital (Royal Devon University Healthcare NHS Foundation Trust). Only patients undergoing mastectomy were approached, as these specimens could be sliced open to allow access to the tumour without affecting subsequent histopathological assessment.

Live subject statement

All experiments were performed in accordance with NHS Health Research Authority (HRA) guidelines, and approved by the North West – Greater Manchester Central Research Ethics Committee (REC). Written informed consents were obtained from human participants of this study.

Following ethical approval (IRAS ID: 210732, study title: Raman spectroscopy for rapid analysis of pathology of the breast) eligible patients received information about the study at least 24 hours before their operation. Informed consent was then obtained in the morning of their surgery.

Once the specimen was removed, the surgeon located the tumour and sliced the specimen to bisect it, allowing access to the tumour surface for measurement, as seen in Fig. 1. The sample was relocated to a nearby room in the theatre block for Raman measurements. The specimen was only kept for measurement for a maximum of 20 minutes before being returned to the theatre and re-entered into the standard sample pathway to pathology assessment.

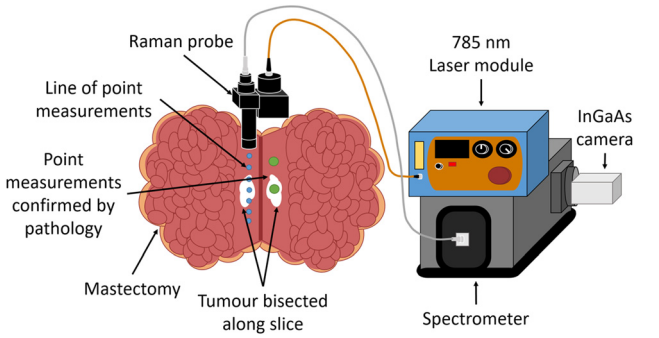

Fig. 1 Experimental set up. Raman spectra were taken using a handheld surface probe with 785 nm wavelength laser, providing 325 mW power with a 1.6 mm beam diameter at the sample surface. Light was collected through a 7 × 105 μm bundle to the spectrometer – Kaiser Holospec – coupled to an iDus InGaAs camera (Andor). Point measurements were taken in a line along the slice in the mastectomy specimen (blue dots) with step sizes of either 0.5 or 1 cm depending on specimen size. Single point measurements were taken on 'tumour' and 'normal' tissue respectively (green dots) for confirmation with pathology.

Raman instrumentation

A diagram of the experimental setup is shown in Fig. 1. Raman measurements were taken using a homebuilt handheld surface probe, connected to a 785 nm laser (Innovative Photonic Solutions, USA) and a Kaiser Holospec spectrometer with a 785 nm edge (Semrock 50 mm Edgebasic® Long wave pass) filter (Kaiser optical systems inc, Ann Arbour, USA) with an InGaAs camera (iDus InGaAs 1.7 μm, Andor, Belfast, UK). The use of the combination of laser and InGaAs camera enabled sensitive detection of the high wavenumber region, not possible with silicon-based CCDs at this wavelength. The probe design contains a 105 μm core fibre, a collimating lens and then a 785 nm laser bandpass filter (Semrock Maxline®), with collimated light then passing through a 785 nm dichroic mirror (Thorlabs, NJ, USA). A 12.5 mm diameter plano-convex f = 20 mm lens with anti-reflective coating (Thorlabs, NJ, USA) was used along with a 20 mm spacer tube, producing a 325 mW beam at the sample with spot size at the focus measured with a beam profiler to be 1.6 mm in diameter. The end of the spacer was placed in contact with the sample when measurements were taken, maintaining the optical working distance required by the f = 20 mm lens that collected the scattered light. This ensured optimum collection at all times when in contact with the tissue. As the spacer was a tube, any pressure applied to the periphery of the region of interest had no effect on the central region measured. Elastically scattered light was rejected by the dichroic filter (Semrock 785 nm) and a 785 nm edge filter (Semrock Razoredge® longpass) before the remaining inelastically scattered light was focused into a multimodal low OH fibre bundle 7 × 105 μm core (Thorlabs BFL105LS02) with round array at one end translating into a linear array, enabling the array to be efficiently launched into the spectrometer mounted with a 100 μm slit. Calculations based on the optical configuration showed the optical collection area to be from a 0.64 mm spot on the surface of the sample. Note the mismatch in the illumination and collection areas, resulting in a range of spatially offset signals (~0.5 mm to 1.1 mm offsets[50]), likely to result in a range of signals collected from the surface and tissue depths of up to ~1 mm. We have tested the instrument with a number of scenarios using lard/protein rich tissue phantoms and demonstrated that protein rich tissues can only be probed when lightly buried by lipid rich materials. From this, we have ascertained that the maximum depth for detection of epithelial tissue beneath adipose tissues to be ~1 mm with the current set up. Furthermore, phantom tumours, within a lipid rich volume, with a surface area between 0.5 and 1 mm^2 were detectable with this set up.[51] Spectra were collected across the region from 0 to 4000 cm^{-1}, but the HWN region from 2500 to 4000 cm^{-1} was focused on in data analysis.

Raman measurement protocol

Approved laser local rules were followed at all times. Before specimen measurements took place, paracetamol was measured as a calibration standard, with 1 s exposure time, and the wavenumber axis was corrected using a polynomial fit. A line of point measurements was taken along the specimen slice, with step sizes of either 0.5 or 1 cm depending on specimen size. Additional single point measurements were taken on 'tumour' and 'normal' tissue respectively, and were indicated with black and blue ink respectively for confirmation with pathology. For each point measurement on the specimen, 3 spectra were taken, each with 5 s exposure time. The number of measurements taken for each specimen varied, with the aim being to maximise the number of measurements possible within the allocated timeframe.

Histopathological examination

Each of the inked measurement locations were assessed by histopathology through routine haematoxylin and eosin (H&E) stained sections taken from larger tissue blocks of the measured locations. The pathologist's assessment of the status of the examined tissue – tumour or normal – and the type of tissue in the surrounding area (fat, stroma, *etc.*) was collated.

Data analysis

Data analysis was carried out using MATLAB (Mathworks, 2018a).

Pre-processing. Firstly, from the full dataset collected, saturated spectra, or spectra with inadequate signal to noise (S : N) levels (S : N < 10), were removed. All remaining spectra were pre-processed before analysis, starting with the subtraction of a spectrum taken with the laser switched off to remove fixed pattern noise. A median filter was then used to remove cosmic rays, then data was baselined to remove background signal, and then normalised; for visualisation and ratio calculations, data were normalised to the CH peak at 2935 cm^{-1}, and for multivariate analysis data were vector normalised.

Groupings. Data was assessed in different groups. These groups were:

- The data validated by histopathology only (194 spectra)
- All data from all measurements (1620 spectra)
- A reduced dataset including data assessed by pathology and data from the line spectra originating from only the most extreme tumour and normal locations (770 spectra).

It is important to clarify that only the first data group contained spectra from tissue that had all been fully validated by histopathology. The second group containing all spectra consists of all pathology validated spectra as well as the rest of the spectra for which the ground truth could only be estimated by the surgeon at the time of measurement. The final, reduced dataset was included to minimise some potential experimental errors, described as follows. In some cases, the tumour was difficult to access based on its location within the specimen, so it is unclear whether the tumour had been directly measured by Raman without precise histopathological validation, and so these measurements were removed from this dataset. Also, the surgeon's indication of the tumour was an estimate, and the exact location was difficult to ascertain in the moment of measurement. Therefore, in the reduced dataset, measurements were retained when there was confi-

dence that they were centred on tumour or benign tissue and the data from the less certain boundary regions was removed to minimise incorrect assignments.

Analysis. For the different data groupings, the mean normal *vs*. mean tumour spectrum, along with respective standard deviations were found, as well as the ratio of the area under the water band to the area under the total HWN region (water to total area ratio – WTAR), as previously described.[43,47] Analysis of line measurements involved assessing the WTAR and position of the CH peak maximum for each measurement point along the line. Multivariate analysis utilising the HWN region of the spectrum was then employed to explore the use of supervised classification models based on the data for prediction of pathology (class). The data was pre-processed as outlined above and principal component analysis (PCA) was employed first, in order to identify the areas of highest variance within the spectra. Analysis of Variance (ANOVA) statistical testing was used to determine the statistically significant principal components (PCs). The PC scores were then used in combination with the 'known' pathology at the location (class) of the measurement to calculate a linear discriminant model (LDA), which plots the values along a new axis which maximises the separation between the classes, while minimizing the variation within classes.

Results and discussion

Fig. 2 shows several images of areas of histological haematoxylin and eosin (H&E) stained sections. These sections were taken from the positions that were inked on the specimen following Raman measurement for the purpose of matching the Raman spectra with the correct pathology of the measured area. Figures (a) and (b), and figures (c) and (d) respectively, show tumour and benign tissue from the same specimen. (a) Depicts invasive ductal carcinoma while (b) shows the normal fibroadipose tissue from another area on the specimen. (c) Is also an image of invasive ductal carcinoma, this time with sclerotic stroma, and (d) is an example of benign fibrocystic change. Invasive ductal carcinoma was the most commonly pathology measured in this study, with a number of cases of invasive lobular carcinoma, and some with mixed types, and small numbers of rarer types. These include one case of pleomorphic lobular carcinoma, shown in (e), and one case of solid papillary carcinoma, shown in (f).

In total, 1620 spectra were analysed – 1051 normal, and 569 tumour. Fig. 3 shows the mean and standard deviation of the normal *versus* tumour HWN spectra for each of the dataset groupings described in the methods; (a) accounts for the histopathology confirmed spectra, (194 spectra), (b) accounts for all spectra, including those confirmed by histopathology (1620), and (c) the reduced dataset, (770 spectra). The band between 3000–3700 cm^{-1} forms as a convolution of several peaks, largely attributed to water.[52] There was a significant difference in the WTAR between normal *vs*. tumour in the histopathology confirmed data (normal *vs*. tumour 0.26 *vs*. 0.68; $p < 0.001$), full dataset (normal *vs*. tumour; 0.29 *vs*. 0.62; $p < 0.001$) and reduced dataset (normal *vs*. tumour 0.24 *vs*. 0.68; $p < 0.001$), as per Fig. 3). This indicates that tumour tissue has increased water content compared to normal tissue, as expected based on the literature. Although not universal, normal breast tissue is more likely to have a higher proportion of adipose tissue to fibrous tissue whilst tumour tissue is more likely to have a higher proportion of protein rich fibrous stroma, which is

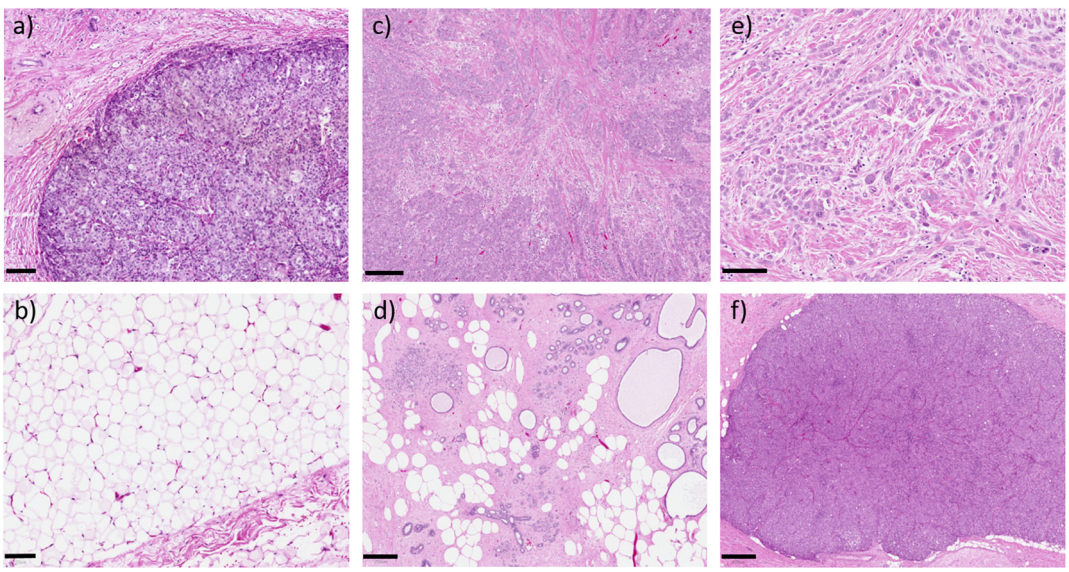

Fig. 2 Example H&E stained breast tissue, where Raman measurements were taken and assessed by histopathology (a) invasive ductal carcinoma, scale bar 100 μm; (b) normal fibroadipose tissue, from the same specimen as (a), with scale bar 100 μm; (c) invasive ductal carcinoma with sclerotic stroma, scale bar 250 μm; (d) benign fibrocystic change, from the same specimen as (c), scale bar 250 μm; (e) pleomorphic lobular carcinoma, scale bar 100 μm; (f) solid papillary carcinoma, scale bar 400 μm.

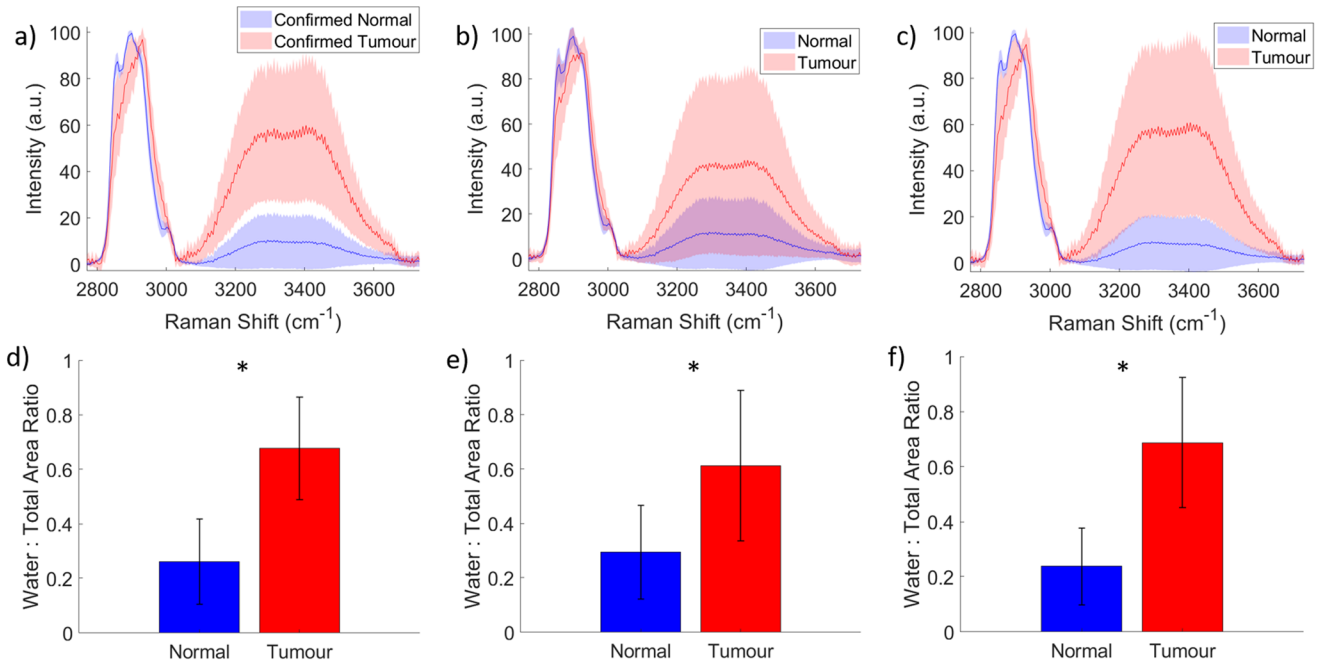

Fig. 3 Mean and standard deviation of normal *versus* tumour spectra. (a) All spectra assessed by histopathology (194 spectra) and reclassified based on this; (b) all spectra (1620 spectra); (c) spectra from reduced dataset (770 spectra); (d), (e) and (f) are bar graphs of the Water to Total Area Ratio (WTAR) of the normal and tumour spectra from figures (a), (b) and (c) respectively; * indicates a statistically significant difference between normal and tumour ($p < 0.001$).

more associated with a high water content.[53] Tumours in general also have a higher density of cells than normal tissue and this tends to mean an increased water content. This is because diffusion is impeded in tissues with high cellularity, meaning water is trapped within cells, as evidenced by diffusion-weighted MRI studies.[54] There are two visible maximum points across the water band, at around 3299 cm^{-1} and 3391 cm^{-1} on average between the three datasets, which are associated with differences in the binding status of water.[52,55] In this region, water peaks at lower wavenumbers indicate a higher degree of intramolecular hydrogen bonding, whereas higher wavenumbers indicate more free water.[52,55] That said the picture is complicated by the fact that there is an N–H stretch contribution to the signals at around 3300 cm^{-1} originating from proteins found in the tissues, so those areas with higher protein density will have a stronger peak in a similar location to that originating from OH stretch affected by higher intramolecular hydrogen bonding.[56] In the normal spectra in this figure, the two maxima are similar in intensity, if very slightly higher at the lower wavenumber peak, unlike in the tumour spectra, where there is a slight increase in the higher wavenumber peak. This could potentially indicate a slightly higher concentration of free water, or only partially bound water in the tumour tissue compared to the normal (although some of this will be driven by the NH stretch contribution). In support of this, a study by Chung *et al.* using broadband DOS found that malignant breast tissue contains significantly higher free water compared to normal tissue.[57] A possible explanation for this, as well as for the higher water content of tumour tissue in general is the influence of angiogenesis. Vessels formed through this process are inefficient and leak plasma, amongst other substances, into the surrounding tissue.[58]

The other important difference between the two spectra is the position of the peak between 2800 cm^{-1} and 3040 cm^{-1}. The normal spectra have prominent peaks at 2859 cm^{-1} and 2900 cm^{-1}, which account for CH_2 lipid stretching, and 3002 cm^{-1}, CH lipid stretching, with a maximum at the 2900 cm^{-1} peak. By contrast, in this region the tumour spectrum has a peak located at 2931 cm^{-1}, attributable to protein CH_2 stretching.[59] The reduction of lipids and increase in protein in the tumour tissue is supported by the literature,[41,46] although for measurements that did not have the histopathological confirmation obtained, it is possible that normal fibroglandular tissue could have been measured in some cases. However, importantly the trend for separation based on both water and protein content is evident specifically in Fig. 3(a), for which the Raman measurements were coupled with histopathological assessment. Furthermore, this shows that the Raman spectra of normal tissue is significantly different from the tumour, confirming the ability of HWN Raman spectroscopy to detect cancer in freshly excised breast tissue.

The differences seen between the mean spectra can be used to indicate the location of a tumour within a specimen as demonstrated in Fig. 4. This figure demonstrates the change in water content and fat/protein content across a line of measurements taken along a single specimen slice and indicates the position of the tumour as estimated by the surgeon.

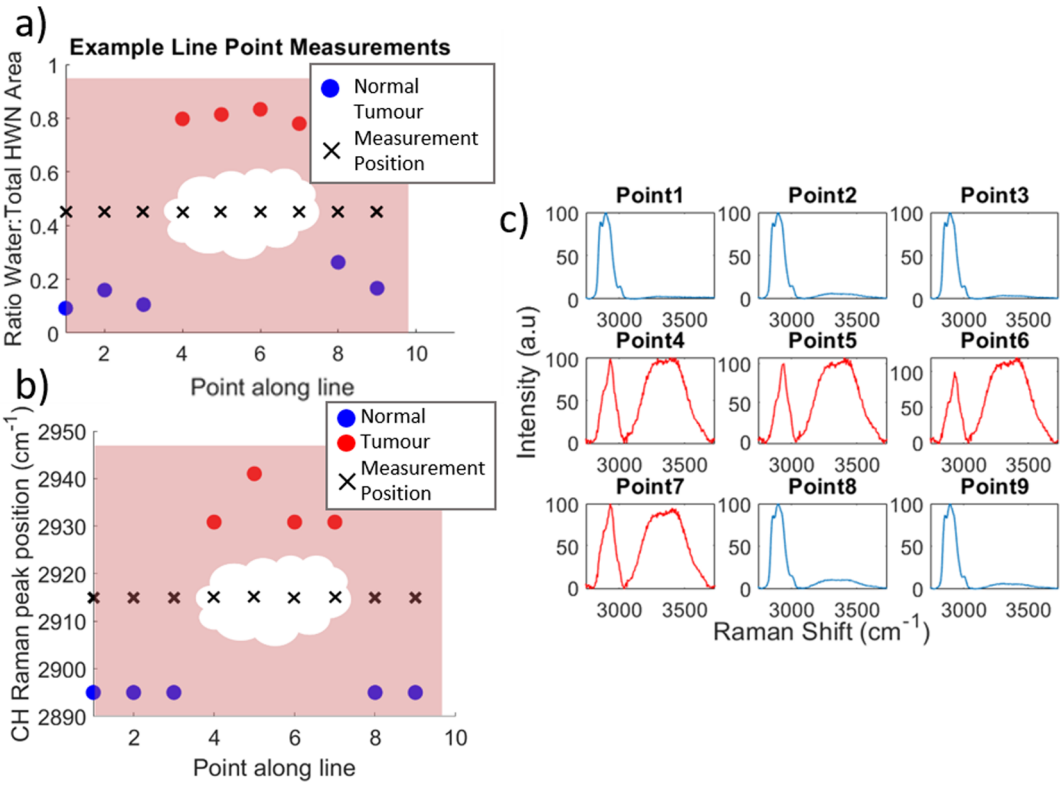

Fig. 4 Water content and CH peak position of spectra from point measurements along lines on a single specimen; (a) ratio of the area under the water band to area under the whole HWN spectrum at each point (red/blue circles) with the physical measurement location along the specimen slice indicated by black crosses and the surgeon's estimate of tumour position indicated by the central white mass; (b) equivalent plot of CH peak position (red/blue circles) with physical measurement location (black crosses) and estimated tumour position (white mass); (c) mean spectra for each point along the line of measurements.

Fig. 5 by contrast shows the data from another line of measurements, line 2, taken from the same specimen but at a distance from the tumour. At each measurement position, for both Fig. 4 and 5, the WTAR and wavenumber at which the maximum of the CH peak is located is plotted in (a) and (b) respectively, with the corresponding mean spectrum for each point shown alongside in (c). In Fig. 4, the tumour position can be clarified by the locations where the WTAR and CH peak

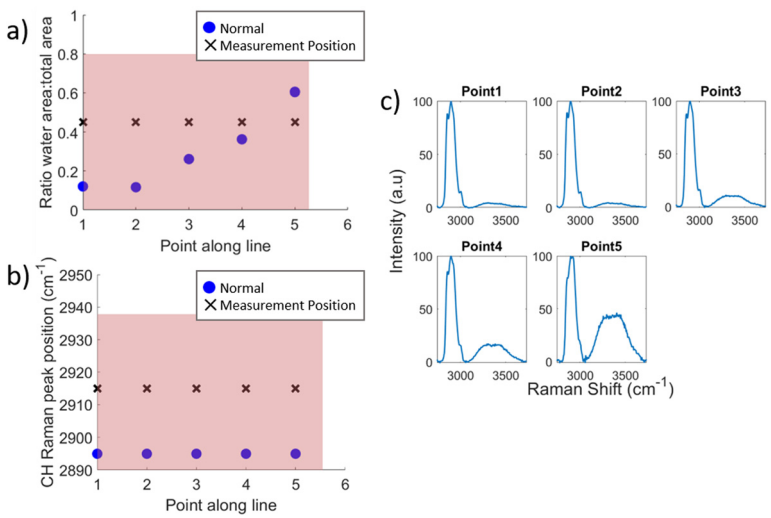

Fig. 5 (a) ratio of the area under the water band to area under the whole HWN spectrum at each point measurement location along the line of point measurements along normal tissue away from specimen slice; (b) equivalent plot of CH peak position; (c) mean spectra for each point along the line of measurements.

position are highest. For this particular specimen, the WTAR for measurements of the tumour are consistently around 0.8, with the average at 0.81. By contrast, the normal measurements for this line have an average WTAR of 0.12. In terms of CH peak position, this is located at a higher wavenumber for the tumour measurements compared to the normal; 2933.5 cm^{-1} compared to 2895 cm^{-1} respectively. In Fig. 5, the CH position of line 2, away from the tumour, also remains stable at 2895 cm^{-1}. The average WTAR for this line, 0.29, is higher than that of the normal points in Fig. 4 but is still much reduced compared to the values obtained from tumour measurements. However, the values do increase towards the end of the line, but are still reduced compared to the tumour measurements, indicating some levels of variation in the WTAR amongst normal tissue.

While this figure shows a very clear distinction between normal and tumour measurements across this particular specimen, this was not necessarily the case for all. That said, it should be noted that these measurements were not assessed by histopathology and the tumour location was an estimate by the surgeon based on palpation and visual assessment, and there is also dependence on the depth of the slice into the tumour. The reduced dataset accounts for this somewhat in that spectra from boundary regions were removed to minimise incorrect assignment, but this does not explain all of the variation. Fig. 6 shows bar graphs indicating the mean WTAR (Fig. 6(a)) and CH peak position (Fig. 6(b)) for normal (blue), boundary (yellow) and tumour (red) positions from the line measurements taken on each specimen, with the standard deviation as the error bars. Looking at the mean values, for the majority of specimens both the WTAR and CH peak wavenumber of tumour measurements is higher than that of normal measurements. This is true for 19/30 specimens in terms of the WTAR and 17/30 in terms of CH peak position. This increases to 20/30 specimens when considering those specimens whose boundary measurements are increased compared to normal. Importantly, there are three specimens where there was either no normal tissue or no tumour tissue measured, and thus not allowing this comparison. In the remaining 27, almost half of the specimens demonstrate a trend where the WTAR or CH position of normal measurements < boundary < tumour. While this is not always the case, this indicates an incremental increase in WTAR and CH position between normal tissue and within the threshold of the tumour. This has been demonstrated by Barroso *et al.* on oral tissue.[45] On average across all specimens, the WTAR was 0.26 for normal, 0.32 for boundary and 0.50 for tumour. The CH position was on average 2901 cm^{-1} for normal, 2903 cm^{-1} for boundary and 2916 cm^{-1} for tumour. It is important to note that for both metrics there can be large variation across individual specimens, as well as variation between patients, as base levels of tissue water content is different for each individual.[60]

Yet, there are a small number of specimens that demonstrate a higher WTAR or CH peak position for normal tissue rather than tumour or boundary tissue. A possible explanation for this is that there may be contributions from dense glandular tissue which, has higher protein and water content than fibroadipose tissue.[53,60] This could also be a factor in the increase in WTAR and broadening of the CH peak seen in the measurements at the end of the line in Fig. 5. While the

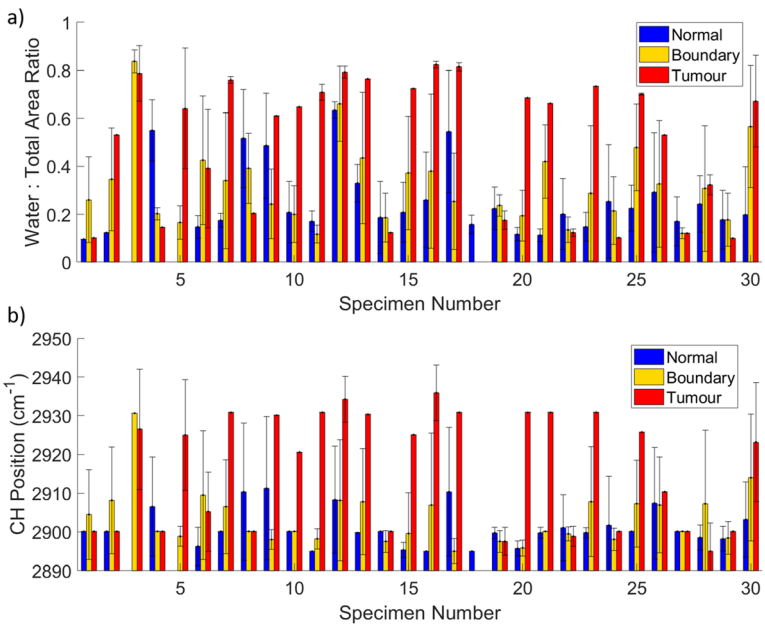

Fig. 6 Water content of point measurements and CH peak position of spectra from point measurements along lines on all specimen; (a) WTAR at each point measurement location along the line of point measurements taken across the length of the specimen slice for each specimen; (b) equivalent plot of CH peak position; bars indicate the mean value of normal (blue), boundary (yellow), and tumour measurements (red), with error bars indicating the standard deviation.

maximum CH peak position did not change, the increase in intensity at 2921 cm^{-1} is indicative of protein.[59] In addition, fat is much more highly scattering than protein, so if there were a small amount of protein-rich tissue in amongst fatty tissue in these measurement locations the lipid signal would still dominate. Also, tumour cells can exhibit discrete single cell invasion resulting in a very low tumour cellularity within tissue predominantly composed of fat.[61]

As seen in Fig. 3(b) and (c) there is some degree of overlap in the standard deviations of both the water band and the CH peak between normal and tumour spectra. This overlap is explored in Fig. 7, which shows normal *vs.* tumour HWN spectra with varying concentrations of fat and stroma in the former, and tumour cells in the latter, as estimated by the pathologist from the histology-assessed dataset. In this figure levels of a specific tissue type are described as 'high' or 'low'; 'high' refers to an estimate of greater than or equal to 50% concentration of that tissue type in the section examined by the pathologist in the vicinity of the Raman point measurement, and 'low' refers to less than 50% of that tissue type. The spectra shown are the mean of the spectra designated as high/low of the particular tissue type, and the standard deviation is shown in the shaded area. As it was not possible to control the levels of fat or stroma in the human samples, spectra taken from areas of tissue determined to be 'high' in one and simultaneously 'low' in the other were used. Across all four plots, it is clear that spectra with high levels of tumour have the highest mean water content, as well a more consistent shift towards 2931 cm^{-1} in the CH peak. Fig. 7(a) shows the opposite is true for normal spectra which are highly fatty; having little to no water content and a very well defined lipid CH peak at 2900 cm^{-1}, these spectra are easily separated from spectra with high tumour levels. The same can be said for the means of the spectra in Fig. 7(b), but the spectra with low tumour levels have a much larger standard deviation, likely owed to contributions from other normal tissue types amongst tumour cells in the area measured. Also, the shifted CH peak is not as well defined and has higher variation. Therefore, while highly fatty normal spectra will be largely distinguished from material with low tumour cell concentration, it is possible that some spectra will be misclassified. A similar conclusion can be drawn from the comparison between high tumour and high stroma normal spectra in Fig. 7(c). Although the mean spectra are sufficiently separate in terms of both the water content and the CH peak position, there is some overlap in the standard deviations, meaning some spectra could be misclassified. To note, the CH peak in the normal spectrum with high stroma is still indicative of the presence of lipids, but shows no or minimal indication of the presence of protein. But, as seen in Fig. 5, this is somewhat expected due to the signal from lipids being much more intense than that from proteins (lipids generate more Raman scattering than a similar concentration of protein molecules). Furthermore, Fig. 7(d) indicates where the biggest classification problem arises, in comparing high stroma normal spectra with low tumour spectra. While the latter still has higher water content on average, the water content of the mean normal spectrum is very close to this, and their standard deviations completely overlap, indicating that this situation is the most likely for incorrect classification to occur. Therefore, if the concentration of tumour cells reduces towards the boundary of the tumour with normal tissue, this could be problematic when it comes to detecting tumour margins. Likewise, with tumours whose cells are particularly infiltrative in nature, this may again limit the detection of these cells.

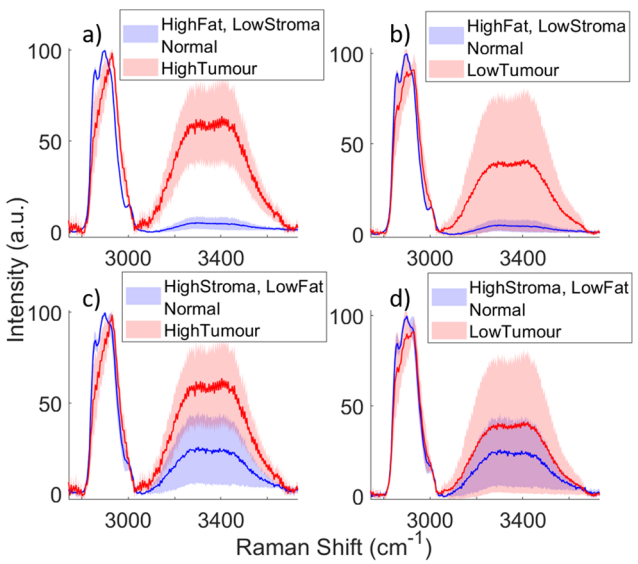

Fig. 7 Comparing the HWN spectra of normal spectra high in fat or stroma to tumour spectra with high or low levels of tumour cells. Here, 'high' refers to a concentration of the particular tissue type of greater than or equal to 50%, as estimated by the pathologist, within the area of the tissue section where Raman spectra was taken. Plotted are the mean and standard deviation of the specific tissue type spectra. (a) Spectra of highly fatty normal tissue (66 spectra) plotted alongside highly concentrated tumour spectra (41 spectra); (b) spectra of highly fatty normal tissue plotted alongside spectra with a low concentration of tumour cells (30 spectra); (c) spectra of normal tissue with a high concentration of stroma (18 spectra) plotted alongside highly concentrated tumour spectra; (d) spectra of normal tissue with a high concentration of stroma plotted alongside spectra with a low concentration of tumour cells.

Fig. 8 demonstrates the classification of the spectra into 'tumour' or 'normal' through the PCA–LDA model. The model uses the reduced dataset, where tumour-normal boundary measurements were excluded, to minimise errors in training the model. Fig. 8(a) Shows the loadings of PC1, PC2 and PC3, which were the most significant PCs based on ANOVA testing ($p < 0.001$). From the statistical testing PC1 is clearly the most significant, demonstrating that the highest variation within the data was a strong lipid CH peak with reduced contributions from the water band. PC2 illustrates the significance of a shift in the CH peak towards higher wavenumbers along with a pronounced increase in signal from water. PC3 relates a reduction in lipid contributions with an increase in the water contribution above 3400 wavenumbers. It should be noted that the region of the spectrum defined here as that relating to the OH stretch of the water also includes some signal form NH

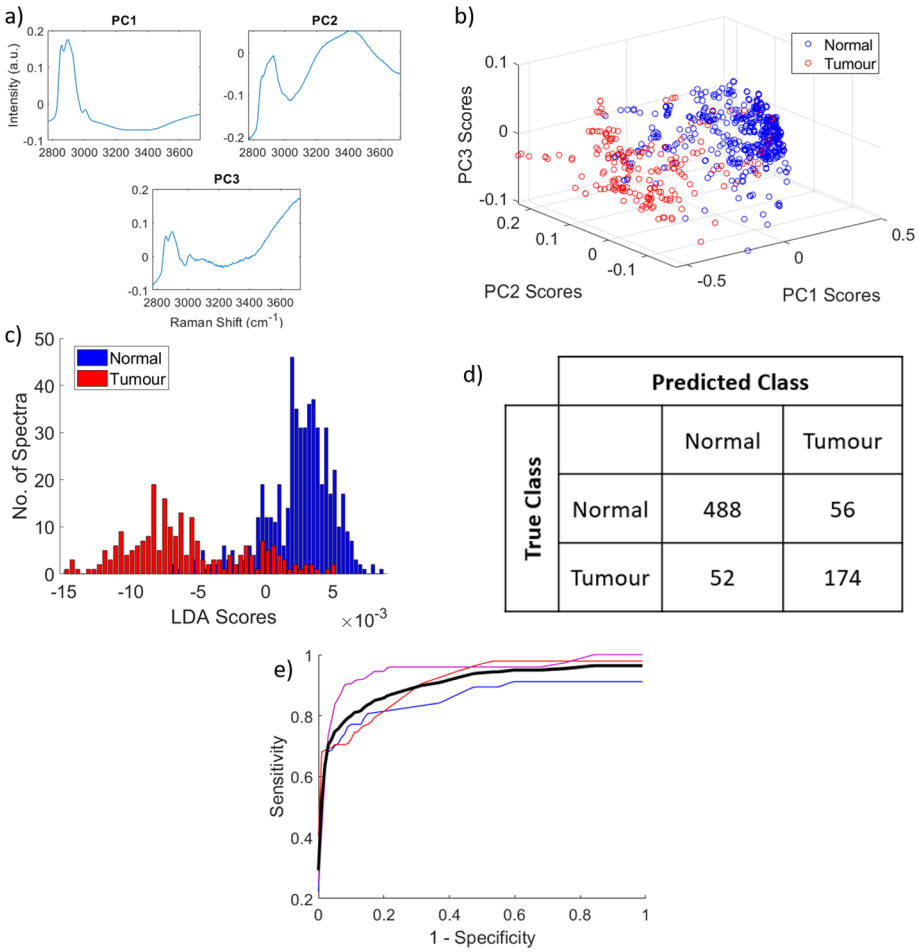

Fig. 8 PCA–LDA classification model. (a) The loadings of PC1, PC2 and PC3; (b) scatter plot of principal component scores from PC1, PC2 and PC3, with normal in blue tumour in red; (c) histogram of the linear discriminant scores; those of normal spectra shown in blue (544 spectra), while those of tumour spectra are shown in red (266 spectra); (d) confusion matrix showing the number of spectra correctly and incorrectly classified as normal and tumour based on the model following leave one sample out cross validation; (e) 3-fold cross validated ROC curve, the red, blue and magenta lines showing each iteration, and black showing the mean, with area under the mean curve of 0.8993.

stretch at 3300 cm^{-1}. The scores of PCs 1, 2 and 3 are plotted against each other in a scatter graph in Fig. 8(b) and this shows good separation between normal and tumour. This is evident again in Fig. 8(c) – a histogram of the subsequent LDA scores. Above zero is a large concentration of normal spectra, with tumour spectra distributed mostly below zero. The tumour spectra are spread much further across the axis indicating the increased heterogeneity of these spectra compared to normal. The specific numbers of correctly and incorrectly classified spectra based on this model are shown in the confusion matrix in Fig. 8(d). Following leave-one-patient-out cross validation, of 544 normal spectra, 488 were correctly classified as normal, and only 56 were misclassified as tumour. Of 226 tumour spectra, 174 were correctly classified as tumour, while 52 were incorrectly classified as normal. This equates to a sensitivity of 77.1%, specificity of 90.8% and overall accuracy of 86.0%, and area under the mean ROC curve following 3-fold cross validation of 0.8993. For completeness a model using data from just the CH region (2800–3000 cm^{-1}) of the spectra, where the difference in lipid and protein rich tissues are most apparent, was also used. This resulted in sensitivity and specificity of 76.1% and 91.7% respectively following leave-one-patient-out cross validation.

Conclusion

This study demonstrates the ability of HWN Raman spectroscopy to distinguish between cancerous and normal breast tissue from freshly excised human samples. The key factors enabling this are the difference in water content, including a potential difference in the behaviour of bound and free water, and fat/protein within normal *versus* tumour, which this technique is able to detect and utilise for classification *via* multivariate modelling. To advance this line of research towards use for intraoperative margin assessment, it is important that the precision of this method is interrogated further. This could be achieved by having a pathologist present for the Raman

measurements, and measuring smaller samples, perhaps in the form of a micro-tissue array. Overall, this work highlights that this method can achieve the fundamental classification of tumour *versus* normal on clinically relevant breast samples, and that it has great potential for future development towards intraoperative margin assessment.

Author contributions

Jennifer Haskell – data curation, formal analysis, investigation, methodology, project administration, resources, software, validation, visualization, writing – original draft, review and editing. Thomas Hubbard – investigation, methodology, project administration, resources, software, writing – review and editing. Claire Murray – investigation, methodology, resources, writing – review and editing. Benjamin Gardner – software, writing – review and editing. Charlotte Ives – resources. Douglas Ferguson – resources, supervision, editing. Nick Stone – conceptualization, formal analysis, funding acquisition, methodology, project administration, resources, software, supervision, validation, writing – review and editing.

Conflicts of interest

There are no conflicts of interest to declare.

Acknowledgements

This work was funded by the EPSRC, grant number EP/P012442/1 and the University of Exeter funded the PhD studentship of J. Haskell who is first author. Thanks go to all the staff in the surgical department of the Royal Devon and Exeter hospital, especially breast surgeons Rachel Tillett, Sisse Olsen and Hannah Knight, as well as Tanwen Wright in the pathology department, and research nurses Linda Park and Tania Nightingale. Thanks also to Pavel Matousek at Rutherford Appleton Laboratory for the valuable discussions.

References

1 B. Fisher, M. Bauer, R. Margolese, R. Poisson, Y. Pilch, C. Redmond, *et al.*, Five-Year Results of a Randomized Clinical Trial Comparing Total Mastectomy and Segmental Mastectomy with or without Radiation in the Treatment of Breast Cancer, *N. Engl. J. Med.*, 1985, **312**(11), 665–673, DOI: 10.1056/NEJM198503143121101.

2 W. S. Schain, M. E. Dunn, A. S. Lichter and L. I. Pierce, Mastectomy versus Conservative Surgery and Radiation Therapy Psychosocial Consequences, *Cancer*, 1994, **73**(4), 1221–1228 https://acsjournals.onlinelibrary.wiley.com/doi/10.1002/1097-0142.

3 S. K. Al-Ghazal, L. Fallowfield and R. W. Blamey, Comparison of psychological aspects and patient satisfaction following breast conserving surgery, simple mastectomy and breast reconstruction, *Eur. J. Cancer*, 2000, **36**(15), 1938–1943.

4 Association of Breast Surgery (ABS), *Association of Breast Surgery Consensus Statement Margin Width in Breast Conservation Surgery*, 2015. Available from: https://www.associationofbreastsurgery.org.uk.

5 N. Houssami, P. Macaskill, M. Luke Marinovich and M. Morrow, The association of surgical margins and local recurrence in women with early-stage invasive breast cancer treated with breast-conserving therapy: A meta-analysis, *Ann. Surg. Oncol.*, 2014, **21**(3), 717–730.

6 S. Downey, L. Chagla, V. Chandran, A. Gandhi, G. Layer and A. Sahu, *et al., Best Practise Guidelines For Surgeons In Breast Cancer Screening*, 2018. https://associationofbreastsurgery.org.uk/media/64276/final-screening-guidelines-2018.pdf.

7 S. S. K. Tang, S. Kaptanis, J. B. Haddow, G. Mondani, B. Elsberger, M. K. Tasoulis, *et al.*, Current margin practice and effect on re-excision rates following the publication of the SSO-ASTRO consensus and ABS consensus guidelines: a national prospective study of 2858 women undergoing breast-conserving therapy in the UK and Ireland, *Eur. J. Cancer*, 2017, **84**, 315–324.

8 KEY PERFORMANCE INDICATORS IN PATHOLOGY Recommendations from the Royal College of Pathologists [Internet], 2013. Available from: https://www.rcpath.org/static/e7b7b680-a957-4f48-aa78e601e42816de/Key-Performance-Indicators-in-Pathology-Recommendations-from-the-Royal-College-of-Pathologists.pdf.

9 T. S. Menes, P. I. Tartter, I. Bleiweiss, J. H. Godbold, A. Estabrook and S. R. Smith, The consequence of multiple re-excisions to obtain clear lumpectomy margins in breast cancer patients, *Ann. Surg. Oncol.*, 2005, **12**(11), 881–885.

10 K. Esbona, Z. Li and L. G. Wilke, Intraoperative imprint cytology and frozen section pathology for margin assessment in breast conservation surgery: A systematic review, *Ann. Surg. Oncol.*, 2012, **19**(10), 3236–3245.

11 T. P. Olson, J. Harter, A. Muñoz, D. M. Mahvi and T. M. Breslin, Frozen section analysis for intraoperative margin assessment during breast-conserving surgery results in low rates of re-excision and local recurrence, *Ann. Surg. Oncol.*, 2007, **14**(10), 2953–2960.

12 J. J. Keating, C. Fisher, R. Batiste and S. Singhal, Advances in intraoperative margin assessment for breast cancer, *Curr. Surg. Rep.*, 2016, **4**(4), 1–8.

13 R. Emmadi and E. L. Wiley, Evaluation of resection margins in breast conservation therapy: The pathology perspective-past, present, and future, *Int. J. Surg. Oncol.*, 2012, **2012**, 180259, DOI: 10.1155/2012/180259.

14 N. Colakovic, D. Zdravkovic, Z. Skuric, D. Mrda, J. Gacic and N. Ivanovic, Intraoperative ultrasound in breast cancer surgery-from localization of non-palpable tumors to objectively measurable excision, *World J. Surg. Oncol.*, 2018, **16**(1), 1–7.

15 J. Schwarz and H. Schmidt, Technology for Intraoperative Margin Assessment in Breast Cancer, *Ann. Surg. Oncol.*, 2020, **27**(7), 2278–2287, DOI: 10.1245/s10434-020-08483-w.

16 L. N. F. Smith, I. T. Rubio, R. Henry-Tillman, S. Korourian and V. S. Klimberg, Intraoperative ultrasound-guided breast biopsy, *Am. J. Surg.*, 2000, **180**(6), 419–423.
17 M. Ramos, J. C. Díaz, T. Ramos, R. Ruano, M. Aparicio, M. Sancho, *et al.*, Ultrasound-guided excision combined with intraoperative assessment of gross macroscopic margins decreases the rate of reoperations for non-palpable invasive breast cancer, *Breast*, 2013, **22**(4), 520–524, DOI: **10.1016/j.breast.2012.10.006**.
18 S. Q. Qiu, M. D. Dorrius, S. J. de Jongh, L. Jansen, J. de Vries, C. P. Schröder, *et al.*, Micro-computed tomography (micro-CT) for intraoperative surgical margin assessment of breast cancer: A feasibility study in breast conserving surgery, *Eur. J. Surg. Oncol.*, 2018, **44**(11), 1708–1713.
19 A. B. E. Attia, G. Balasundaram, M. Moothanchery, U. S. Dinish, R. Bi, V. Ntziachristos, *et al.*, A review of clinical photoacoustic imaging: Current and future trends, *Photoacoustics*, 2019, **16**, 100144, DOI: **10.1016/j.pacs.2019.100144**.
20 I. Kosik, M. Brackstone, A. Kornecki, A. Chamson-Reig, P. Wong and J. J. L. Carson, Lipid-weighted intraoperative photoacoustic tomography of breast tumors: Volumetric comparison to preoperative MRI, *Photoacoustics*, 2020, **18**, 100165, DOI: **10.1016/j.pacs.2020.100165**.
21 Y. Goh, G. Balasundaram, H. M. Tan, T. C. Putti, S. W. Tang, C. W. Q. Ng, *et al.*, Biochemical "decoding" of breast ultrasound images with optoacoustic tomography fusion: First-in-human display of lipid and collagen signals on breast ultrasound, *Photoacoustics*, 2022, **27**, 100377, DOI: **10.1016/j.pacs.2022.100377**.
22 E. R. St John, J. Balog, J. S. McKenzie, M. Rossi, A. Covington, L. Muirhead, *et al.*, Rapid evaporative ionisation mass spectrometry of electrosurgical vapours for the identification of breast pathology: Towards an intelligent knife for breast cancer surgery, *Breast Cancer Res.*, 2017, **19**(1), 1–14.
23 J. M. Dixon, L. Renshaw, O. Young, D. Kulkarni, T. Saleem, M. Sarfaty, *et al.*, Intra-operative assessment of excised breast tumour margins using ClearEdge imaging device, *Eur. J. Surg. Oncol.*, 2016, **42**(12), 1834–1840, DOI: **10.1016/j.ejso.2016.07.141**.
24 M. Thill, C. Dittmer, K. Baumann, K. Friedrichs and J. U. Blohmer, MarginProbe® - Final results of the German post-market study in breast conserving surgery of ductal carcinoma in situ, *Breast*, 2014, **23**(1), 94–96, DOI: **10.1016/j.breast.2013.11.002**.
25 F. Schnabel, S. K. Boolbol, M. Gittleman, T. Karni, L. Tafra, S. Feldman, *et al.*, A randomized prospective study of lumpectomy margin assessment with use of marginprobe in patients with nonpalpable breast malignancies, *Ann. Surg. Oncol.*, 2014, **21**(5), 1589–1595.
26 T. M. Allweis, Z. Kaufman, S. Lelcuk, I. Pappo, T. Karni, S. Schneebaum, *et al.*, A prospective, randomized, controlled, multicenter study of a real-time, intraoperative probe for positive margin detection in breast-conserving surgery, *Am. J. Surg.*, 2008, **196**(4), 483–489.
27 M. Thill, MarginProbe®: Intraoperative margin assessment during breast conserving surgery by using radiofrequency spectroscopy, *Expert Rev. Med. Devices*, 2013, **10**(3), 301–315.
28 A. S. Haka, K. E. Shafer-Peltier, M. Fitzmaurice, J. Crowe, R. R. Dasari and M. S. Feld, Diagnosing breast cancer by using Raman spectroscopy, *Proc. Natl. Acad. Sci. U. S. A.*, 2005, **102**(35), 12371–12376 **https://www.pnas.org/doi/abs/10.1073/pnas.0501390102**.
29 N. Stone, C. Kendall, J. Smith, P. Crow and H. Barr, Raman spectroscopy for identification of epithelial cancers, *Faraday Discuss.*, 2004, **126**, 141–157 **https://pubs.rsc.org/en/content/articlehtml/2004/fd/b304992b**.
30 Z. Huang, A. McWilliams, H. Lui, D. I. McLean, S. Lam and H. Zeng, Near-infrared Raman spectroscopy for optical diagnosis of lung cancer, *Int. J. Cancer*, 2003, **107**(6), 1047–1052.
31 P. Crow, A. Molckovsky, N. Stone, J. Uff, B. Wilson and L. M. Wongkeesong, Assessment of fiberoptic near-infrared raman spectroscopy for diagnosis of bladder and prostate cancer, *Urology*, 2005, **65**(6), 1126–1130.
32 A. S. Haka, Z. Volynskaya, J. A. Gardecki, J. Nazemi, J. Lyons, D. Hicks, *et al.*, In vivo Margin Assessment during Partial Mastectomy Breast Surgery Using Raman Spectroscopy, *Cancer Res.*, 2006, **66**(6), 3317–3322 **https://aacrjournals.org/cancerres/article/66/6/3317/527477/In-vivo-Margin-Assessment-during-Partial**.
33 M. Sattlecker, C. Bessant, J. Smith and N. Stone, Investigation of support vector machines and Raman spectroscopy for lymph node diagnostics, *Analyst*, 2010, **135**(5), 895–901 **https://pubs.rsc.org/en/content/articlehtml/2010/an/b920229c**.
34 J. Horsnell, P. Stonelake, J. Christie-Brown, G. Shetty, J. Hutchings, C. Kendall, *et al.*, Raman spectroscopy—A new method for the intra-operative assessment of axillary lymph nodes, *Analyst*, 2010, **135**(12), 3042–3047 **https://pubs.rsc.org/en/content/articlehtml/2010/an/c0an00527d**.
35 G. R. Lloyd, L. E. Orr, J. Christie-Brown, K. McCarthy, S. Rose, M. Thomas, *et al.*, Discrimination between benign, primary and secondary malignancies in lymph nodes from the head and neck utilising Raman spectroscopy and multivariate analysis, *Analyst*, 2013, **138**(14), 3900–3908 **https://pubs.rsc.org/en/content/articlehtml/2013/an/c2an36579k**.
36 R. Damadian, Tumor detection by nuclear magnetic resonance, *Science*, 1971, **171**(3976), 1151–1153.
37 C. Kiricuta and V. Simplã¤ceanu, Tissue Water Content and Nuclear Magnetic Resonance in Normal and Tumor Tissues, *Cancer Res.*, 1975, **35**, 1164–1167**https://aacrjournals.org/cancerres/article-pdf/35/5/1164/2394055/cr0350051164.pdf**.
38 D. P. Hollis, J. S. Economou, L. C. Parks, J. C. Eggleston, L. A. Saryan and J. L. Czeisler, Nuclear Magnetic Resonance Studies of Several Experimental and Human Malignant Tumors, *Cancer Res.*, 1973, **33**(9), 2156–2160.
39 P. E. Sijens, H. K. Wijrdeman, M. A. Moerland, C. J. G. Bakker, J. W. A. H. Vermeulen and P. R. Luyten,

Human breast cancer in vivo: H-1 and P-31 MR spectroscopy at 1.5 T, *Radiology*, 1988, **169**(3), 615–620.

40 N. R. Jagannathan, M. Singh, V. Govindaraju, P. Raghunathan, O. Coshic, P. K. Julka, *et al.*, Volume localized in vivo proton MR spectroscopy of breast carcinoma: variation of water±fat ratio in patients receiving chemotherapy, *NMR Biomed.*, 1998, **11**, 414–422 https://analyticalsciencejournals.onlinelibrary.wiley.com/doi/10.1002/.

41 A. E. Cerussi, N. S. Shah, D. Hsiang, A. Durkin, J. A. Butler and B. J. Tromberg, In vivo absorption, scattering, and physiologic properties of 58 malignant breast tumors determined by broadband diffuse optical spectroscopy, *J. Biomed. Opt.*, 2006, **11**(4), 044005, DOI: 10.1117/12337546 https://www.spiedigitallibrary.org/journals/journal-of-biomedical-optics/volume-11/issue-4/044005/In-vivo-absorption-scattering-and-physiologic-properties-of-58-malignant/10.1117/1.2337546.full.

42 Y. Qi, R. Zhang, P. Rajarahm, S. Zhang, A. B. Ebrahim Attia, R. Bi and M. Olivo, Simultaneous Dual-Wavelength Source Raman Spectroscopy with a Handheld Confocal Probe for Analysis of the Chemical Composition of In Vivo Human Skin, *Anal. Chem.*, 2023, **95**(12), 5240–5247, DOI: 10.1021/acs.analchem.2c05065.

43 L. E. Masson, C. M. O'Brien, I. J. Pence, J. L. Herington, J. Reese, T. G. Van Leeuwen, *et al.*, Dual excitation wavelength system for combined fingerprint and high wavenumber Raman spectroscopy, *Analyst*, 2018, **143**(24), 6049–6060 https://pubs.rsc.org/en/content/articlehtml/2018/an/c8an01989d.

44 E. M. Barroso, R. W. H. Smits, T. C. B. Schut, I. Ten Hove, J. A. Hardillo, E. B. Wolvius, *et al.*, Discrimination between Oral Cancer and Healthy Tissue Based on Water Content Determined by Raman Spectroscopy, *Anal. Chem.*, 2015, **87**(4), 2419–2426.

45 E. M. Barroso, R. W. H. Smits, C. G. F. Van Lanschot, P. J. Caspers, I. Ten Hove, H. Mast, *et al.*, Water concentration analysis by Raman spectroscopy to determine the location of the tumor border in oral cancer surgery, *Cancer Res.*, 2016, **76**(20), 5945–5953.

46 A. F. García-Flores, L. Raniero, R. A. Canevari, K. J. Jalkanen, R. A. Bitar, H. S. Martinho, *et al.*, High-wavenumber FT-Raman spectroscopy for in vivo and ex vivo measurements of breast cancer, *Theor. Chem. Acc.*, 2011, **130**(4–6), 1231–1238 https://link.springer.com/article/10.1007/s00214-011-0925-9.

47 T. J. E. Hubbard, A. P. Dudgeon, D. J. Ferguson, A. C. Shore and N. Stone, Utilization of Raman spectroscopy to identify breast cancer from the water content in surgical samples containing blue dye, *Transl. Biophotonics*, 2021, **3**(2), e202000023 https://onlinelibrary.wiley.com/doi/full/10.1002/tbio.202000023.

48 H. Abramczyk, B. Brozek-Pluska, J. Surmacki, J. Jablonska-Gajewicz and R. Kordek, Hydrogen bonds of interfacial water in human breast cancer tissue compared to lipid and DNA interfaces, *J. Biophys. Chem.*, 2011, **02**(02), 159–170.

49 Z. Liao, M. G. Lizio, C. Corden, H. Khout, E. Rakha and I. Notingher, Feasibility of integrated high-wavenumber Raman imaging and fingerprint Raman spectroscopy for fast margin assessment in breast cancer surgery, *J. Raman Spectrosc.*, 2020, **51**(10), 1986–1995.

50 S. Mosca, C. Conti, N. Stone and P. Matousek, Spatially offset Raman spectroscopy, *Nat. Rev. Methods Primers*, 2021, **1**(1), 21, DOI: 10.1038/s43586-021-00019-0.

51 T. Hubbard, *Using Raman Spectroscopy for Intraoperative Margin Analysis in Breast Conserving Surgery*, University of Exeter, 2020.

52 C. Choe, J. Lademann and M. E. Darvin, Depth profiles of hydrogen bound water molecule types and their relation to lipid and protein interaction in the human stratum corneum in vivo, *Analyst*, 2016, **141**(22), 6329–6337 https://pubs.rsc.org/en/content/articlehtml/2016/an/c6an01717g.

53 S. J. Graham, S. Ness, B. S. Hamilton and M. J. Bronskill, Magnetic resonance properties of ex vivo breast tissue at 1.5 T, *Magn. Reson. Med.*, 1997, **38**(4), 669–677.

54 Y. Guo, Y. Q. Cai, Z. L. Cai, Y. G. Gao, N. Y. An, L. Ma, *et al.*, Differentiation of clinically benign and malignant breast lesions using diffusion-weighted imaging, *J. Magn. Reson. Imaging*, 2002, **16**(2), 172–178.

55 R. Vyumvuhore, A. Tfayli, H. Duplan, A. Delalleau, M. Manfait and A. Baiilet-Guffroy, Effects of atmospheric relative humidity on Stratum Corneum structure at the molecular level: Ex vivo Raman spectroscopy analysis, *Analyst*, 2013, **138**(14), 4103–4111.

56 P. J. Caspers, G. W. Lucassen, E. A. Carter, H. A. Bruining and G. J. Puppels, In vivo confocal raman microspectroscopy of the skin: Noninvasive determination of molecular concentration profiles, *J. Invest. Dermatol.*, 2001, **116**(3), 434–442, DOI: 10.1046/j.1523-1747.2001.01258.x.

57 S. H. Chung, A. E. Cerussi, C. Klifa, H. M. Baek, O. Birgul, G. Gulsen, *et al.*, In vivo water state measurements in breast cancer using broadband diffuse optical spectroscopy, *Phys. Med. Biol.*, 2008, **53**(23), 6713–6727.

58 S. Ziyad and M. L. Iruela-Arispe, Molecular Mechanisms of Tumor Angiogenesis, *Genes Cancer*, 2011, **2**(12), 1085–1096 https://journals.sagepub.com/doi/full/10.1177/1947601911432334.

59 Z. Movasaghi, S. Rehman and I. U. Rehman, Raman Spectroscopy of Biological Tissues, *Appl. Spectrosc. Rev.*, 2007, **42**(5), 493–541 https://www.tandfonline.com/doi/abs/10.1080/05704920701551530.

60 N. Boyd, L. Martin, S. Chavez, A. Gunasekara, A. Salleh, O. Melnichouk, *et al.*, Breast-tissue composition and other risk factors for breast cancer in young women: a cross-sectional study, *Lancet Oncol.*, 2009, **10**(6), 569–580.

61 P. Friedl and K. Wolf, Tumour-cell invasion and migration: diversity and escape mechanisms, *Nat. Rev. Cancer*, 2003, **3**(5), 362–374 https://www.nature.com/articles/nrc1075.